Investigation of the ternary phase diagram of mechanically alloyed FeCuAg

1997 J. Phys.: Condens. Matter 9 3259

(http://iopscience.iop.org/0953-8984/9/15/016)

J. Phys.: Condens. Matter **9** (1997) 3259–3276. Printed in the UK PII: S0953-8984(97)80675-3

Investigation of the ternary phase diagram of mechanically alloyed FeCuAg

N S Cohen, E Ahlswede†, J D Wicks‡ and Q A Pankhurst

Department of Physics and Astronomy, University College London, Gower Street, London WC1E 6BT, UK

Received 6 January 1997, in final form 11 February 1997

Abstract. The structural and magnetic properties of mechanically alloyed Fe–Cu–Ag at room temperature have been investigated using ^{57}Fe Mössbauer spectroscopy, x-ray diffraction and differential scanning calorimetry. The elements are naturally immiscible, but through prolonged and energetic ball milling (70 hours at 600 rpm) one can make metastable alloys, the structure of which depends on the elemental composition. In the binary Cu–Ag and Fe–Cu systems, crystalline single-phase solid solutions result, whereas in Fe–Ag the alloying is limited, with the product a mixture of elemental particles. In the ternary system it is possible to produce copper- and silver-rich single-phase fcc alloys, but not the equivalent bcc iron-based structure. As the proportions of the three elements become more equal, the resulting structure becomes highly disordered or amorphous. The composition range of this amorphous phase is different to that observed in sputtered Fe–Cu–Ag systems.

1. Introduction

There has been much recent interest in the use of mechanical alloying to produce alloys of otherwise immiscible systems, as it can provide routes to metastable states not otherwise accessible. It also has practical advantages over techniques such as sputtering, vapour deposition and melt quenching, in the large volumes and low costs of sample preparation. The process often employs a ball mill, in which the high-energy impact of hardened balls on the elemental powders induces alloying through repeated fracturing and cold welding.

Two mechanically alloyed binary systems have been a particular focus of both fundamental and applied interest, namely Fe–Cu and Fe–Ag. Mechanical alloying of Fe–Cu produces a range of metastable alloys of these otherwise immiscible elements. Single-phase fcc structures are produced for Cu-rich mixtures whereas a bcc structure results in the Fe-rich case [1, 2]. The Fe–Cu alloys can exhibit interesting nanocrystalline effects and unusual thermodynamic and magnetic properties. In contrast, the Fe–Ag system supports no analogous metastable states, and instead there is incomplete or minimal alloying, even after prolonged milling. The result is a granular structure, where ferromagnetic Fe particles are dispersed in the Ag matrix. These materials are known to exhibit giant magnetoresistive effects, where the electrical resistivity of the material can be markedly altered by the application of a magnetic field [3, 4]. This is of current applied interest, opening up the possibility of an economic mechanical alloying route to the large-scale production of GMR materials for use in, for example, magnetic sensing devices.

† Present address: Fraunhofer-Institut für Angewandte Festkörperphysik, D-79108 Freiburg, Germany.
‡ Present address: Cavendish Laboratory, Madingley Road, Cambridge CB3 0HE, UK.

0953-8984/97/153259+18$19.50

Given the importance of these two binary systems, it is perhaps surprising that there have been no reports to date on mechanical alloying of the ternary Fe–Cu–Ag system. There has been some previous work on sputtered samples [5, 6], but none on mechanically alloyed samples. There are two main reasons for a study of ball-milled Fe–Cu–Ag being of interest. First, the data from the sputtered alloys indicate an amorphous region in the centre of the ternary phase diagram. This represents an intriguing phase change away from the fcc solid solutions of $Cu_{50}Ag_{50}$ and $Fe_{50}Cu_{50}$ and the immiscible bcc-Fe and fcc-Ag constituents of $Fe_{50}Ag_{50}$. A comparison of the nature of this amorphous state as attained by mechanical alloying and by sputtering is therefore valuable, as is the systematic study of the evolution of the amorphous state as a function of elemental composition. Second, there is the question of how the addition of Cu to the Fe–Ag alloy system might affect its microstructure, especially with regard to grain sizes and the related GMR properties. In this case it is not just the as-milled state that is of interest, but also the post-production annealed material. In this context it is possible that a near-homogeneous or amorphous precursor state might be particularly advantageous for the growth of ultrafine Fe grains.

The work presented in this paper is part of a wider research programme directed at an improved understanding of amorphous magnetism, and of the materials properties of Fe-based granular magnets. Here we focus on the structural and magnetic properties of as-milled Fe–Cu–Ag alloys as determined using a combination of ^{57}Fe Mössbauer spectroscopy, x-ray diffraction and differential scanning calorimetry. Mössbauer spectroscopy gives microscopic magnetic and structural information to complement the diffraction results. This is of particular value in this case as it is difficult to separate the diffraction peaks of bcc-Fe from those of fcc-Ag. Additionally, correlations can be made between the magnetic and structural phase diagrams. Differential scanning calorimetry is a useful complementary technique to help in distinguishing between disordered polycrystalline materials and those that are amorphous on a finer scale.

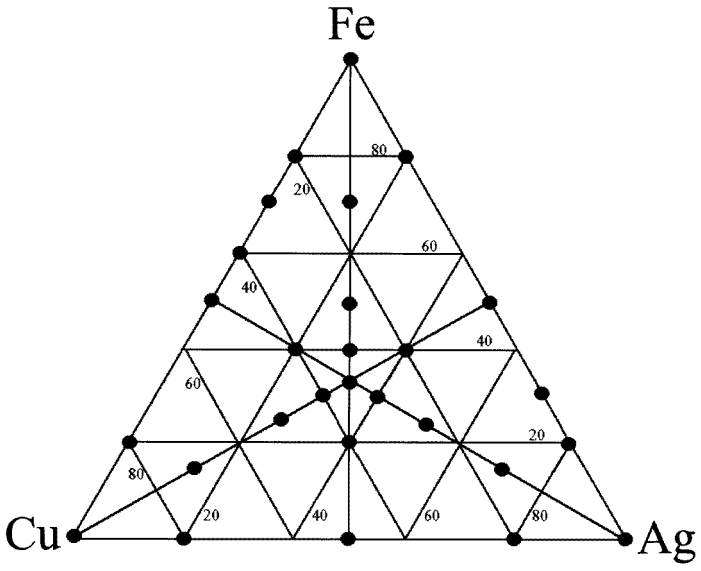

Figure 1. A FeCuAg ternary phase diagram showing the sample compositions that were tested.

Table 1. Mössbauer and x-ray data for the FeCuAg ternary alloy system. The table comprises the Mössbauer isomer shift δ, paramagnetic quadrupole splitting Δ, mean hyperfine field B_{hf}, rms deviation ΔB_{hf} and relative spectral area of the subcomponent spectra, and the lattice parameters a and crystallite sizes d calculated from the x-ray data. All of the data were taken at room temperature, except where indicated. The numbers in parentheses are uncertainties.

Sample	δ (mm s^{-1})	Δ (mm s^{-1})	B_{hf} (T)	ΔB_{hf} (T)	Area	a_{fcc} (Å)	a_{bcc} (Å)	d (Å)
$Cu_{80}Ag_{20}$						3.71(1)		80(5)
$Cu_{50}Ag_{50}$						3.88(1)		60(5)
$Cu_{20}Ag_{80}$						4.00(1)		75(5)
$Fe_{80}Cu_{20}$	0.02(1)	—	31.5(1)	2.4(12)	0.57(14)		2.88(1)	75(5)
	0.08(1)	—	29.4(6)	3.7(18)	0.43(14)			
$Fe_{50}Cu_{50}$	0.10(1)	—	22.2(1)	6.3(32)	0.67(2)	3.63(1)		105(5)
	0.15(1)	0.0 (fixed)	—	—	0.33(2)			
$Fe_{20}Cu_{80}$	0.16(1)	0.47(1)	—	—	1	3.61(1)		115(5)
$Fe_{80}Ag_{20}$	0.02(1)	—	33.5(1)	1.4(3)	0.38(1)		2.88(1)	55(5)
	0.03(1)	—	31.1(1)	4.6(9)	0.58(1)			
	0.08(2)	0.0 (fixed)	—	—	0.04(1)			
$Fe_{50}Ag_{50}$	0.01(1)	—	33.0(1)	1.2(5)	0.62(1)	4.07(1)		60(5)
	0.07(2)	—	30.8(2)	6.9(26)	0.27(1)			
	0.33(3)	0.65(5)	—	—	0.11(1)			
$Fe_{20}Ag_{80}$	0.02(1)	—	33.3(1)	1.4(3)	0.40(6)	4.07(1)		95(5)
	0.04(1)	—	30.8(3)	4.3(23)	0.42(6)			
	0.28(4)	0.0 (fixed)	—	—	0.17(6)			
Fe	0.01(1)	—	32.8(1)	0.6(2)	0.48(1)		2.88(1)	60(5)
	0.05(1)	—	31.1(1)	6.7(12)	0.52(1)			
$Fe_{70}Cu_{15}Ag_{15}$	0.01(1)	—	32.8(1)	1.7(11)	0.28(6)		2.89(1)	50(5)
	0.06(1)	—	31.2(2)	3.7(18)	0.40(6)			
	0.08(1)	—-	28.6(4)	5.6(32)	0.32(6)			
$Fe_{50}Cu_{25}Ag_{25}$	0.05(1)	—	29.6(1)	3.7(15)	0.62(6)	3.97(1)	2.88(1)	25(5)
	0.11(1)	—	25.3(7)	6.4(35)	0.38(6)			
$Fe_{40}Cu_{30}Ag_{30}$	0.07(1)	—	25.2(1)	8.4(20)	0.69(5)		Amorphous	
	0.40(3)	0.30(5)	—	—	0.31(5)			
$Fe_{20}Cu_{40}Ag_{40}$	0.17(1)	0.41(2)	—	—	1			
$Fe_{20}Cu_{40}Ag_{40}$	0.27(2)	—	21.2(4)	1.2(5)	0.90(3)		Amorphous	
at 80 K	0.10(2)	0.64(4)	—	—	0.10(3)			
Cu						3.62(1)		110(5)
$Cu_{70}Fe_{15}Ag_{15}$	0.20(1)	0.49(1)	—	—	1	3.67(1)		70(5)
$Cu_{50}Fe_{25}Ag_{25}$	0.18(1)	0.42(1)	—	—	1	3.71(1)		35(5)
$Cu_{40}Fe_{30}Ag_{30}$	0.15(1)	—	13.8(2)	15.3(50)	1		Amorphous	
$Cu_{20}Fe_{40}Ag_{40}$	0.05(1)	—	28.8(1)	3.5(14)	0.47(5)	4.03(1)		30(5)
	0.10(1)	—	24.1(4)	2.4(12)	0.34(5)			
	0.26(1)	0.35(2)	—	—	0.19(5)			
Ag						4.07(1)		130(5)
$Ag_{70}Fe_{15}Cu_{15}$	0.19(1)	0.43(1)	—	—	0.20(2)	3.98(1)		50(5)
$Ag_{50}Fe_{25}Cu_{25}$	0.24(1)	0.36(1)	—	—	0.23(2)	3.97(1)		40(5)
$Ag_{40}Fe_{30}Cu_{30}$	0.14(1)	—	18.4(1)	10.4(23)	1		Amorphous	
$Ag_{20}Fe_{40}Cu_{40}$	0.09(1)	—	21.3(1)	8.4(21)	0.81(2)	4.02(1)		25(5)
	0.21(3)	0.49(10)	—	—	0.19(2)			
$Fe_{33}Cu_{33}Ag_{33}$	0.10(1)	—	17.6(2)	10.2(35)	1		Amorphous	

2. Experimental details

Twenty-eight different samples were prepared, with compositions chosen to systematically cover the full ternary phase diagram, as shown in figure 1. As well as the end members and binary FeCu, FeAg and CuAg alloys, three series of ternary alloys were prepared: $Fe_{100-2x}Cu_xAg_x$, $Cu_{100-2x}Fe_xAg_x$ and $Ag_{100-2x}Fe_xCu_x$, covering the full range from $x = 0$ to $x = 50$.

The milling was carried out using a Fritsch Pulverisette 7 high-energy planetary ball mill with hardened steel bowls and balls. Approximately 8 g of sample was used in each case, and the bowls were sealed in an inert nitrogen atmosphere. The ball-to-powder mass ratio was approximately 12:1. Some equivalent samples were milled in air for a comparative study on the effect of oxide contamination. A milling velocity of 8 on the control unit was chosen, corresponding to a milling disc rotation frequency of 600 rpm. To prevent excessive heating the mill was operated continuously for two-hour periods, and this was interspersed with cooling down periods of one hour. In this way the mean temperature of the steel bowls and balls was kept at approximately 40 ± 5 °C throughout. Initially, an aliquot of sample was removed for analysis every 10 hours. This enabled the progress of alloying with time to be studied. From these data it was concluded that a total milling time of 60 hours was sufficient to complete the formation of the new phases, where this was possible. Subsequently studied samples were all milled for 70 hours to ensure completion.

Structural analysis was carried out using a Philips X-Pert x-ray diffractometer arranged in θ–θ reflection geometry with molybdenum Kα radiation. Phase analysis, and strain and particle size determinations were performed using the proprietary software on this diffractometer.

^{57}Fe Mössbauer spectra were collected using a constant-acceleration unit arranged in transmission geometry with an unpolarized 50 mCi source of ^{57}Co in a Rh matrix. A triangular drive waveform was used. Data were collected in 576 channels, with $\sim 10^6$ counts per channel, and were folded to remove any baseline curvature. Calibration was with respect to α-iron at room temperature. The spectra were computer analysed using a least-squares fitting program based on a combination of standard methods, including Lorentzian sextets or doublets for the subspectra of magnetically ordered crystalline or paramagnetic phases, and Voigtian sextets for the magnetic amorphous phases. The Voigtian profiles were constrained to have physically realistic and meaningful line positions and linewidths, as described in the model of Lines and Eibschütz [7].

Differential scanning calorimetry (DSC) measurements were made using a Perkin–Elmer DSC7 instrument operating from room temperature to between 500 and 650 °C at a heating rate of 20 °C per minute. Samples of mass ∼20 mg were placed in open platinum pans, and the experiments were performed in a nitrogen atmosphere flowing at a rate of 20 ml min^{-1}.

Selected x-ray diffraction and Mössbauer data for the binary alloys and the three ternary alloy series are summarized in table 1 and in figures 2 to 5. These results are discussed in sections 3, 4 and 5. The DSC data are presented and discussed in section 6.

3. The effect of milling on pure Fe, Cu and Ag

As a preliminary study, the three elements were milled separately and changes in their physical appearance and structure investigated. The initial crystallite size was ∼300–500 Å as calculated from the minimal line broadening in their XRD patterns. After 70 hours' milling there were characteristic changes in both the crystallite size and the bulk physical state. The crystallite size significantly decreased in all three cases, as was evident from

the relatively broad XRD lines (compared to those for the unmilled samples), as shown in figures 3, 4 and 5. Comparison of the XRD pattern of the milled iron (figure 3) with the milled copper and silver shows that it has the broadest lines of the three. This is confirmed in the results of linewidth analysis, which determined crystallite sizes of order 60 Å for iron, 110 Å for copper and 130 Å for silver. Further XRD data, including lattice parameters, are given in table 1. The bulk form of the milled iron was that of loose fine particles, micrometres in scale, whereas that of the silver was that of large aggregates, millimetres in size, which adhered to the surface of the milling balls.

These observations can be explained by considering the effects of the local heat generation at the collision and impact sites during the milling process. Simultaneously with the crystal fracturing and creation of dislocations and grain boundaries that result from the high-energy impacts, this heating will encourage additional processes normally associated with annealing, such as reduction in lattice strain, recrystallization, grain growth and particle agglomeration. These effects are most pronounced in silver, which has the lowest melting point and heat of formation, and least so in iron which has the highest. Thus the silver crystallites have a larger size than the iron crystallites, and tend to agglomerate rather than remain separate.

The Mössbauer spectrum of the milled pure iron, shown in figure 3, is quite different from that of the unmilled powder. The latter is a single sextet with hyperfine field $B_{\mathrm{hf}} = 32.9$ T and narrow lines, corresponding to a small root mean square deviation in B_{hf} relative to the mean, $\Delta B_{\mathrm{hf}} = 0.5$ T. The spectrum of the milled sample was modelled as two sextets, one with $B_{\mathrm{hf}} = 32.8$ T and $\Delta B_{\mathrm{hf}} = 0.4$ T, and a second with $B_{\mathrm{hf}} = 31.1$ T and $\Delta B_{\mathrm{hf}} = 4.4$ T. These two subspectra may be regarded as approximating a broad range of disturbed local environments for the iron atoms, ranging from relatively unchanged (the $B_{\mathrm{hf}} = 33.0$ T subspectrum) to significantly distorted (the $B_{\mathrm{hf}} = 31.0$ T subspectrum), with the large linewidths indicative of the degree of local disorder. This disorder is most likely to take the form of lattice defects, dislocations and lattice distortions which, as well as being formed during the milling process, are volumetrically more significant in the 60 Å crystallites.

It is interesting to note that the Mössbauer spectrum observed here after high-energy milling for 70 hours is different from that reported for a pure iron sample milled in a conventional cylinder ball mill for 2000 hours [8]. In the conventionally milled sample the distribution in hyperfine fields extends to lower values, and the 'valleys' between the absorption peaks do not return to the level of the baseline. At first sight this implies that the conventionally milled sample is in some way 'more disordered' than our high-energy milled sample, which is strange given the lower collision energies available in the conventional mill. However, Tanaka *et al* noted that in their sample milled for 2000 hours there was some contamination, with approximately 5 at.% carbon, 15 at.% oxygen and 0.4 at.% nitrogen in the product [8]. It is possible that these impurities, incorporated into the iron, could account for the different Mössbauer spectrum.

4. Binary alloys

4.1. Copper–silver

Both copper and silver have face-centred cubic structures, but as seen from their equilibrium phase diagram [9] they are naturally immiscible in all but minute proportions at room temperature. This is due to the mismatch in the atomic sizes, with the metallic radius of silver being 13% greater than that of copper.

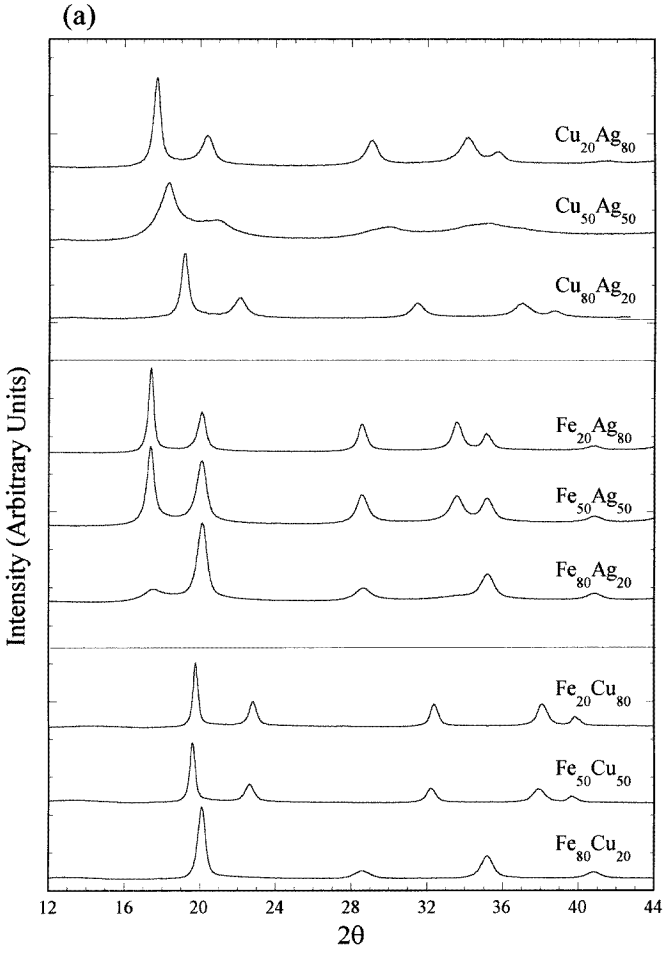

Figure 2. (a) X-ray diffraction patterns of the binary CuAg, FeCu and FeAg systems prepared by mechanical alloying. For clarity all data have been normalized to the same maximum relative intensity. (b) Room temperature Mössbauer spectra of the FeCu and FeAg alloys. The solid lines are least-squares fits of the data, as discussed in the text.

However, it was found that the energy from the heavy plastic deformation and fracturing processes which occur during mechanical alloying are sufficient to overcome the positive enthalpy of mixing and create a full substitutional solid solution that is continuous across the composition range. The lattice parameter of the resultant alloy as calculated from the XRD peak positions increases with the addition of the larger silver atoms in accordance with Vegard's law; the results are summarized in figure 2 and table 1. Additionally, whereas the XRD scans of $Cu_{80}Ag_{20}$ and $Cu_{20}Ag_{80}$ showed sharp, well defined peaks, that of $Cu_{50}Ag_{50}$ showed much broader peaks indicative of a more disordered structure.

The metastable nature of the alloy is highlighted by its rapid decomposition into separate silver and copper clusters after annealing at 250 °C for one hour (data not shown). Further evidence for this metastability was found in milling experiments performed in air, rather than in nitrogen. It was found that the presence of atmospheric oxygen was sufficient to prevent alloying. Evidence of the initial stages of solid-solution formation was seen after five hours,

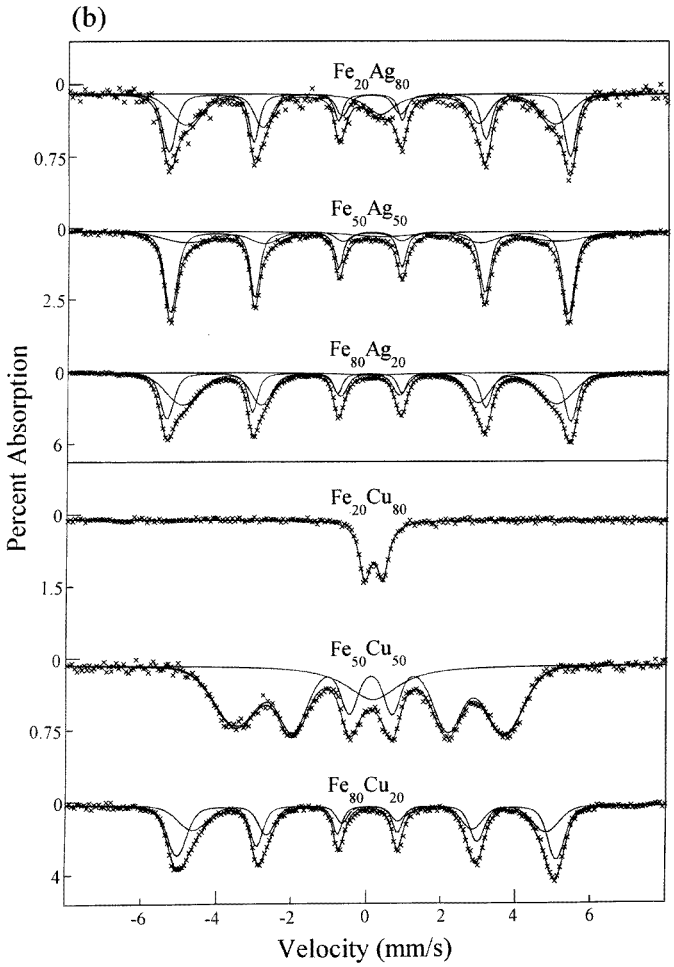

Figure 2. (Continued)

with characteristic shifts in the XRD peak positions, but with extended milling copper oxide compounds were formed in preference, with the silver reverting to its unalloyed state.

4.2. Iron–copper

The iron–copper binary system differs from that of copper–silver in that a change of phase on the part of one of the constituents would be involved in order to create a solid-solution alloy, i.e. between bcc (iron) and fcc (copper). However, in this case the radii of iron and copper are similar, with that of iron being the smaller by only 1.5%, and thus little change in the lattice parameter would be expected in the product.

The mechanically alloyed system has been widely studied and our results confirm those of previous investigators. The evolution of structure with milling time [1, 10], its variation with composition [1, 2], the magnetic properties [11–13] and the effects of annealing [14, 15] have all been reported. In our work, after 70 hours' milling, iron and copper form a solid solution, which has either an fcc, bcc or mixed structure depending on the exact

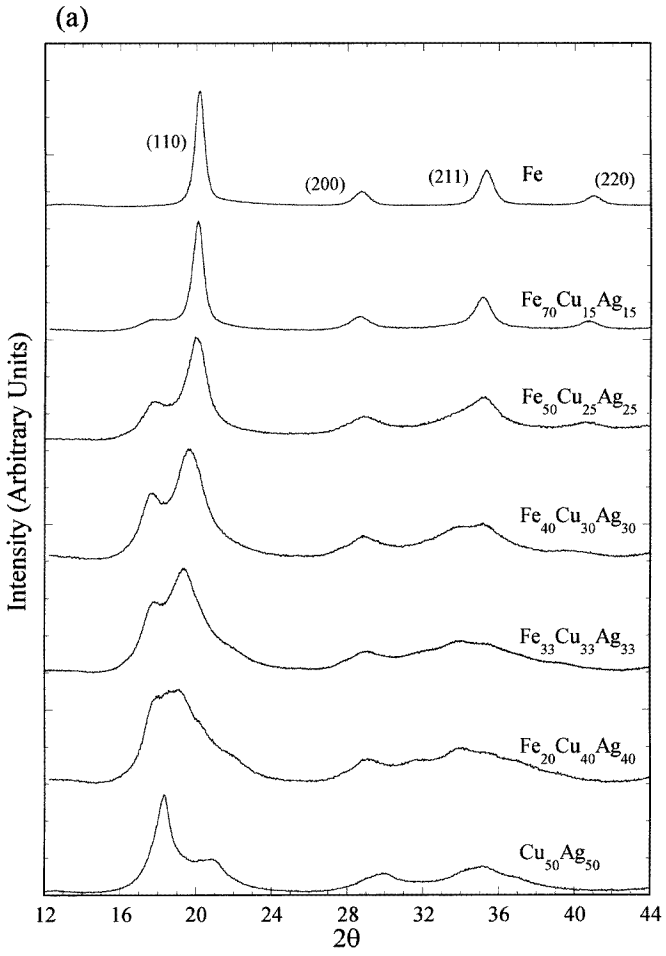

Figure 3. (a) X-ray diffraction patterns of the ternary system $Fe_{100-2x}Cu_xAg_x$ for $x = 0$, 15, 25, 30, 33.3, 40 and 50. All scans have been normalized to the same maximum relative intensity. (b) Room temperature Mössbauer spectra of the $x = 0$, 15, 25, 30, 33.3 and 40 alloys. The solid lines are least-squares fits of the data, as discussed in the text.

composition. Data are shown in figure 2 and table 1.

$Fe_{80}Cu_{20}$ has both XRD and Mössbauer patterns which are very similar to those of milled bcc iron, although the Mössbauer spectrum has slightly reduced hyperfine-field values indicating that the iron and copper are mixed on an atomic level. $Fe_{70}Cu_{30}$ is within the region of transition between the bcc-iron-based and fcc-copper-based phases, and both types of structure are apparent within the XRD pattern, although the bcc phase is dominant. The transition is complete when the composition has reached $Fe_{60}Cu_{40}$. X-ray analysis of $Fe_{50}Cu_{50}$ shows that the structure is fcc, with a lattice parameter of 3.63 Å, close to that of standard copper. However, the Mössbauer spectrum shows the sample to be ferromagnetic, with a mean hyperfine-field value of 22.2 T, and with a small additional paramagnetic component which can be attributed to isolated iron atoms embedded in the copper. A more precise fit of this spectrum [16] constructs the ferromagnetic component from several sextet subcomponents and models the various possible combinations of iron and copper nearest-

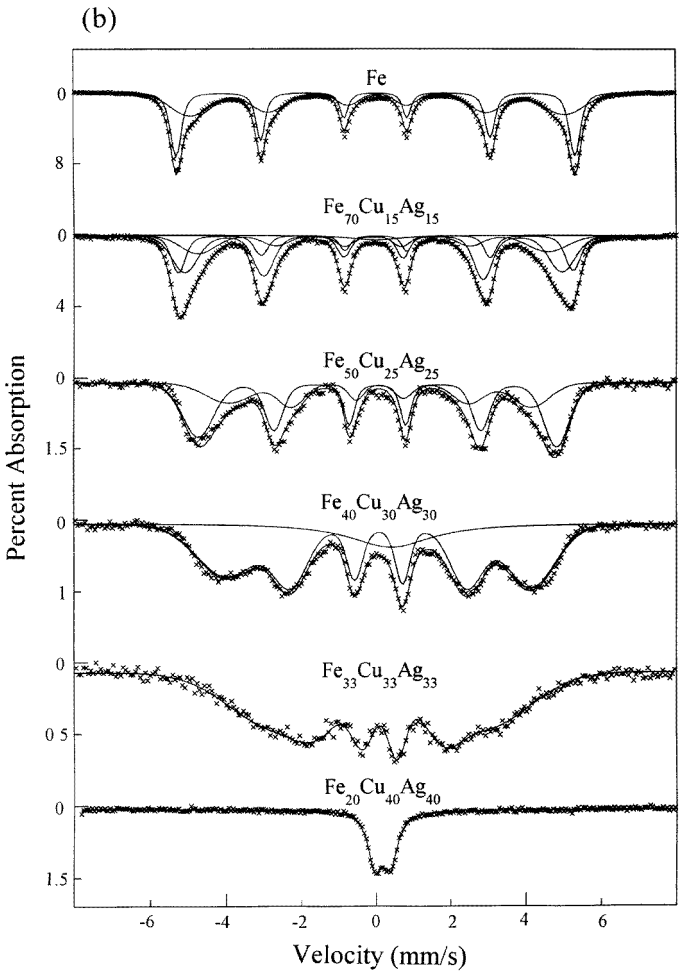

Figure 3. (Continued)

neighbour atoms which would exist in a random substitutional solid solution. $Fe_{20}Cu_{80}$ is again an fcc structure like that of copper, but is paramagnetic, indicating that the iron atoms are widely dispersed in the lattice. There is little change in the lattice parameter of the fcc alloy with composition, which is expected given the similarity in radii of the two components.

4.3. Iron–silver

The solubility of iron in silver is the lowest of the three binary mixtures [17]. This is expected given the 15% difference in the metallic radii of the two elements together with the necessity for a phase transformation by one of them to enable solid-solution formation. Even after 70 hours' milling, only minimal alloying was found. This contrasts with the results from sputtered samples [18] where single-phase alloys were obtained, which were either of a bcc- or fcc-type structure depending on composition.

In the XRD patterns (figure 2) it is not possible to separate out the peaks which

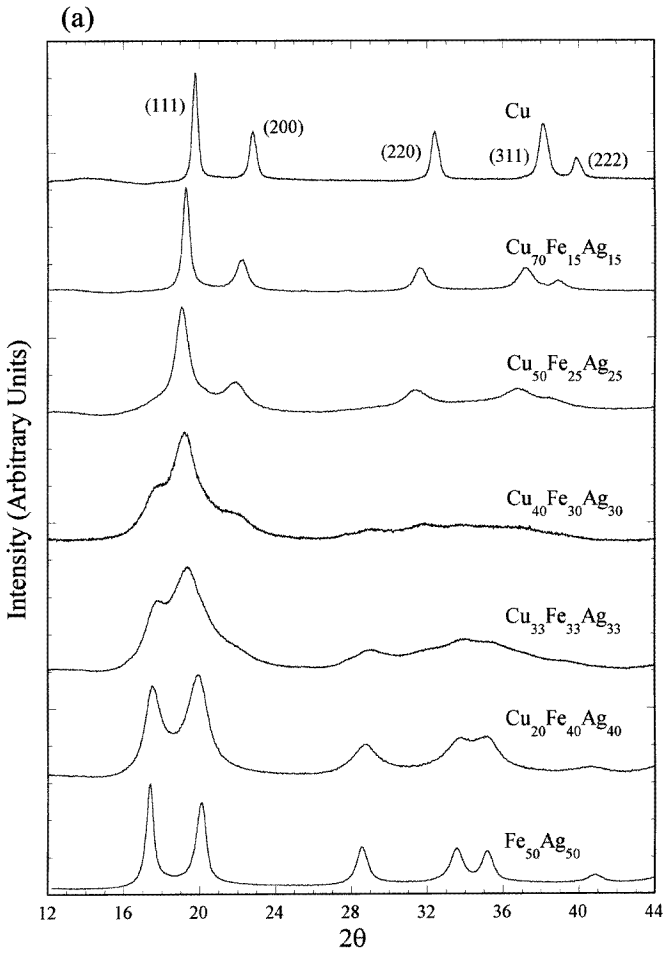

Figure 4. (a) X-ray diffraction patterns of the ternary system $Cu_{100-2x}Fe_xAg_x$ for $x = 0$, 15, 25, 30, 33.3, 40 and 50. All scans have been normalized to the same maximum relative intensity. (b) Room temperature Mössbauer spectra of the $x = 15$, 25, 30, 33.3, 40 and 50 alloys. The solid lines are least-squares fits of the data, as discussed in the text.

correspond to iron from those due to silver. However, there is a change in the relative intensity across the composition range of the two main peaks, the first being Ag(111) and the second a superposition of Ag(200) and Fe(110). The Ag(111) peak remains visible even in the $Fe_{80}Ag_{20}$ mixture. This, together with the fact that there is no change in peak position as a result of milling, indicates that the two elements remain separate. Using the Scherrer formula to analyse the broadening of the Ag(111) peak, an estimate of 60–90 Å is made for the individual crystallite sizes in all three samples.

The Mössbauer spectra confirm this analysis, although at first sight (see figure 2) it may seem curious that the $Fe_{80}Ag_{20}$ and $Fe_{20}Ag_{80}$ spectra are similar, with two overlapping sextets, while the $Fe_{50}Ag_{50}$ spectrum is almost entirely comprised of a single sextet. In all three spectra the sextet with sharper lines has a hyperfine field of order 33 T, indicating that it is due to Fe atoms in a bulk bcc iron environment, i.e. inside α-Fe crystallites. The $Fe_{80}Ag_{20}$ spectrum corresponds to that seen for the milled pure iron, with the broadened

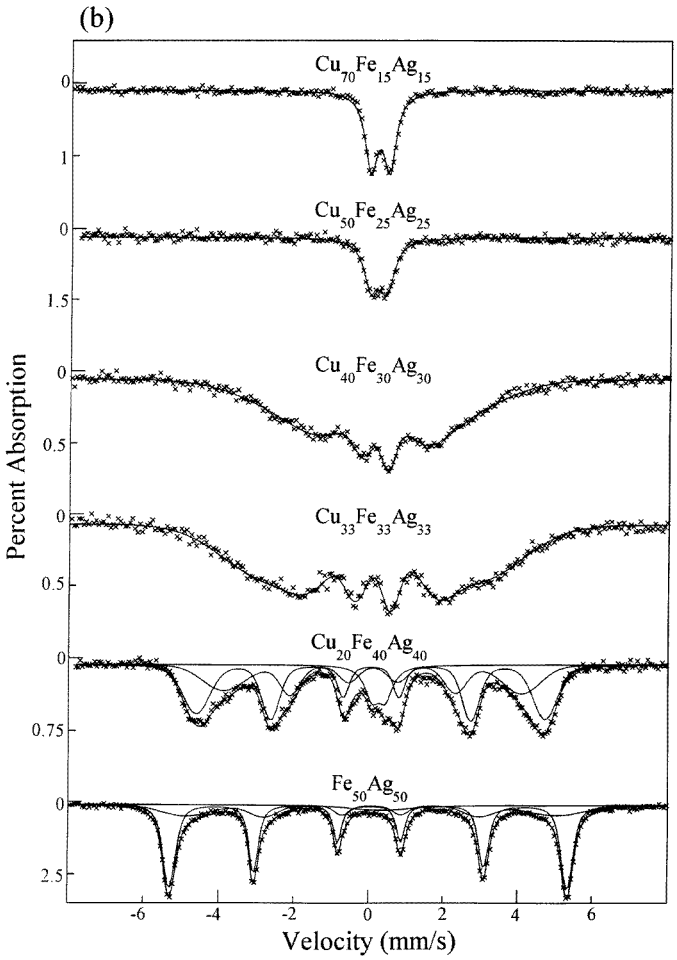

Figure 4. (Continued)

second sextet having the same parameters (see table 1) as in the pure nanocrystalline iron.

The $Fe_{50}Ag_{50}$ spectrum is dominated by the α-Fe sextet, with a minor component, $\sim$30% by area, ascribed to a second sextet with broad lines and reduced hyperfine field. This result is comparable to that reported in the literature for a sample of $Fe_{50}Ag_{50}$ that was milled in a conventional low-energy mill for 800 hours [19], where the broadened component was attributed to limited Fe–Ag mixing to form a solid solution at the grain boundaries. The relative number of atoms which occur at the interface may be estimated as follows. If we assume that the Fe atoms occur in spherical crystallites of diameter d, surrounded by a spherical shell of thickness t which is half occupied with Fe atoms and half with Ag atoms, then the ratio of the number of Fe atoms in the shell compared to the total number of Fe atoms in the core and the shell is the same as the ratio of volumes, $R = (1 - x^3)/(1 + x^3)$, where $x = d/(d + 2t)$. For the $Fe_{50}Ag_{50}$ sample the Mössbauer data give $R \approx 0.30$, so if $d \approx 60$ Å as determined from the x-ray data, then $t \approx 7$ Å, corresponding to a notional two or three monolayers of mixing on the crystallite surface.

The $Fe_{20}Ag_{80}$ sample can be understood similarly, with the broad sextet with $B_{hf} \approx$

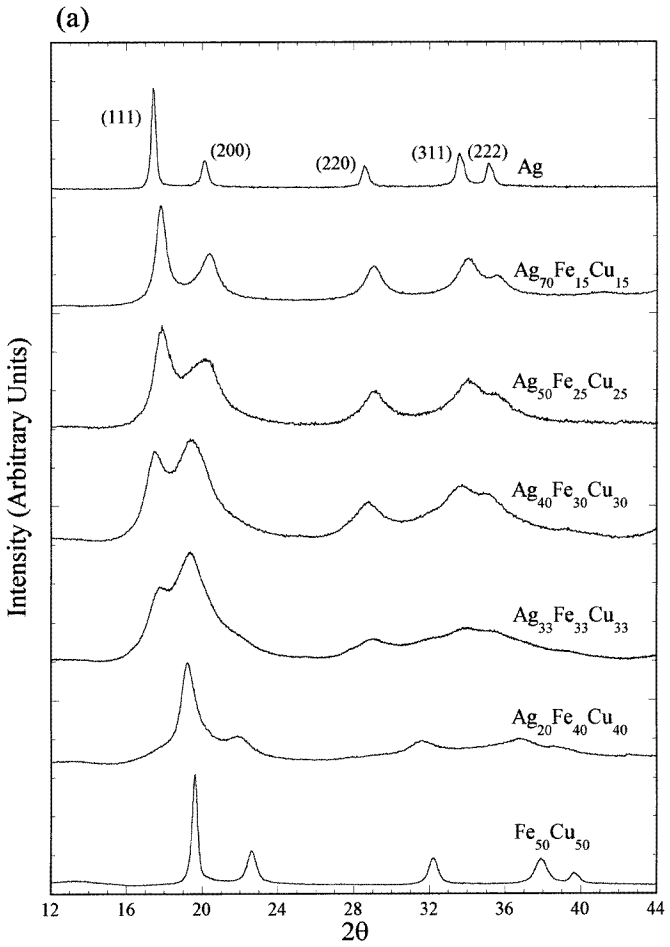

Figure 5. (a) X-ray diffraction patterns of the ternary system $Ag_{100-2x}Fe_xCu_x$ for $x = 0$, 15, 25, 30, 33.3, 40 and 50. All scans have been normalized to the same maximum relative intensity. (b) Room temperature Mössbauer spectra of the $x = 15$, 25, 30, 33.3, 40 and 50 alloys. The solid lines are least-squares fits of the data, as discussed in the text.

30.5 T corresponding to interfacial mixing between the iron and silver. An additional small central absorption is also apparent, indicating that a few isolated iron atoms have entered the fcc silver lattice. In this case $R \approx 0.51$ is the area ratio of the broad sextet to the sum of the broad and sharp sextets. Using $d \approx 95$ Å from the x-ray data gives $t \approx 22$ Å. This is a surprisingly large surface mixing layer, and may be a misleading result. Strictly speaking the x-ray data on crystallite size pertain to the silver grains only, as the overlap of the silver and iron XRD peaks makes it difficult to reliably estimate the iron grain size. It is quite possible that the iron grains are actually smaller than the silver grains, given our earlier results on milling the pure elements. If we assume that we would still expect that a surface shell of thickness $t = 7$ Å would surround any iron particle, the diameter required to give $R = 0.51$ is $d \approx 31$ Å. This is a reasonable figure.

The structure across the iron–silver binary system is thus one where there is a high level of mixing of elements rather than true atomic scale alloying. This feature has already been

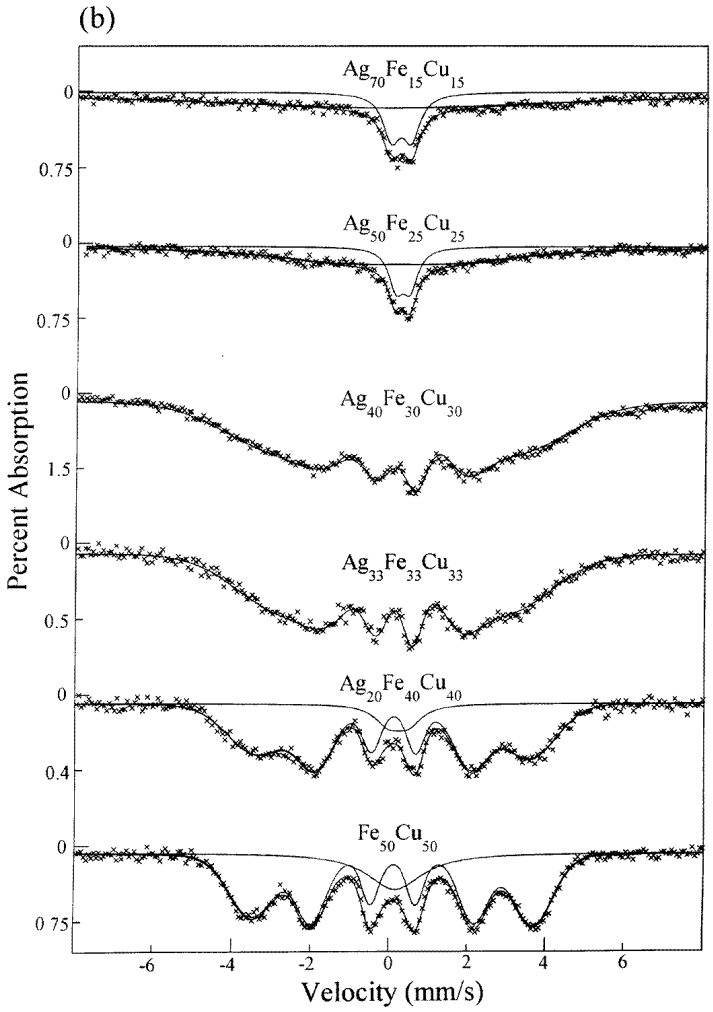

Figure 5. (Continued)

identified in alloys such as $Fe_{20}Ag_{80}$ as leading to potential application as granular giant magnetoresistive materials [3, 13], as it fulfils the basic requirements of having ultrafine ferromagnetic particles dispersed in a non-magnetic conducting matrix. We are currently conducting separate experiments measuring the magnetoresistive properties of these alloys.

5. The FeCuAg ternary system

X-ray and Mössbauer data for $Fe_{100-2x}Cu_xAg_x$, $Cu_{100-2x}Fe_xAg_x$ and $Ag_{100-2x}Fe_xCu_x$ are shown in figures 3, 4 and 5. Systematic trends are apparent in all three series. The x-ray patterns become very broad in the vicinity of the $Fe_{33}Cu_{33}Ag_{33}$ composition at the centre of the phase diagram, inferring either a highly disordered or amorphous state. For the $Cu_{100-2x}Fe_xAg_x$ and $Ag_{100-2x}Fe_xCu_x$ series the alloys on either side of $Fe_{33}Cu_{33}Ag_{33}$ have sharper XRD lines, implying less disordered or more crystalline states. In the

$Fe_{100-2x}Cu_xAg_x$ series there is evidence for extensive disorder at compositions other than the central point, especially for $Fe_{20}Cu_{40}Ag_{40}$, which has an almost featureless diffraction pattern.

Trends are also seen in the Mössbauer data. There is a consistent decrease in the hyperfine field B_{hf} as the proportion of iron in the alloy decreases, with alloys with less than ∼25 at.% Fe giving a paramagnetic doublet spectrum. Increasing distributions in B_{hf} are evident from substantial line broadening for samples near the central composition region. The spectrum of the $Fe_{33}Cu_{33}Ag_{33}$ sample is especially broad, and there is no sign of any crystalline-phase absorption peaks. This spectrum is similar to the broad and featureless spectra of amorphous alloy ribbons [20], and can be very well modelled using the Lines and Eibschütz model for amorphous metals. Computer fits using this model are shown in figures 3, 4 and 5. Taken together with the x-ray data this represents strong evidence that those alloys near the central point of the phase diagram are amorphous, although as will be seen in section 6 the DSC data for these alloys raise a question regarding the length scale of the amorphicity.

The results for several specific regions of the composition range are worthy of particular interest. These are discussed below.

5.1. Silver-rich and copper-rich alloys: fcc paramagnets

Fcc, paramagnetic ternary alloys form in both the silver-rich and copper-rich corners of the phase diagram. The diffraction pattern of $Fe_{15}Cu_{70}Ag_{15}$ (figure 4) is that of an fcc-type material based on copper. The lattice parameter of 3.67 Å is larger than the 3.63 Å for pure copper, and marks the alloying of the metals. The Mössbauer spectrum is a paramagnetic doublet showing that the iron is dispersed within the fcc lattice.

For $Fe_{15}Cu_{15}Ag_{70}$ (figure 5) the evidence that it is a single-phase fcc alloy comes from the Mössbauer spectrum rather than the diffraction data. This is because, as with the binary Fe–Ag alloys, small-intensity bcc-Fe peaks may be masked by the strong fcc-Ag peaks. The Mössbauer spectrum is a paramagnetic doublet, consistent with iron atoms well dispersed in a fcc lattice, as in $Fe_{20}Cu_{80}$, and unlike the bcc-Fe ferromagnetic sextet of $Fe_{20}Ag_{80}$. The diffraction data do, however, show a small shift in the peak positions towards higher angles, from which a lattice parameter of 3.98 Å can be calculated, compared to 4.07 Å for pure silver. This is consistent with a modification of the silver lattice by the addition of copper. Thus a silver-rich fcc alloy containing iron can be produced on adding a small amount of copper, whereas a pure AgFe fcc alloy could not be made by milling.

5.2. Iron-rich alloys: mixed-phase ferromagnets

In the iron-rich corner of the phase diagram a single-phase bcc alloy of iron, copper and silver could not be produced through milling, despite the ease with which the metastable bcc iron–copper solid solution was formed. The diffraction pattern of $Fe_{70}Cu_{15}Ag_{15}$ (figure 3) is dominated by the characteristic reflections of iron, but small peaks from silver are clearly visible, indicating that, while there may have been some degree of alloying, perhaps involving the copper, the resulting sample is not a single-phase alloy. The Mössbauer spectrum is a broadened sextet with parameters similar to those of $Fe_{80}Cu_{20}$, implying that the copper atoms are present in the iron crystallites.

5.3. Equi-proportioned FeCuAg alloys: amorphous ferromagnets

There is no definite transition point between an ordered and disordered structure as the composition is varied. However, it is possible to mark a region of the diagram, central but offset slightly towards low iron concentration, within which the structures tend towards disorder. Amorphous alloys, as evident from Mössbauer spectra that can be described as single-component Lines and Eibschütz-type profiles, are identified in figures 3, 4 and 5 as those which have only one solid line superimposed on the data points. These are the alloys $Fe_{33}Cu_{33}Ag_{33}$, $Fe_{30}Cu_{30}Ag_{40}$ and $Fe_{30}Cu_{40}Ag_{30}$.

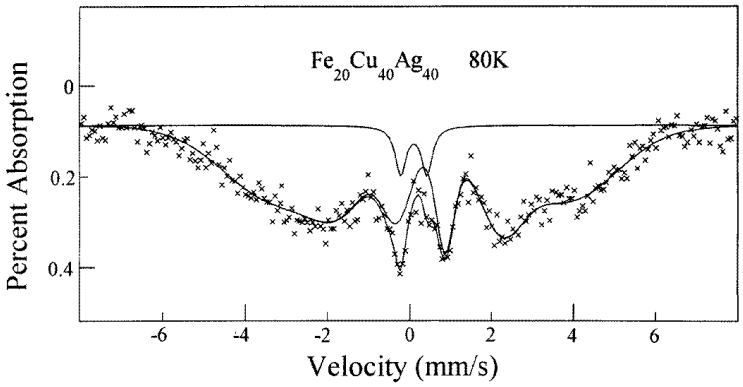

Figure 6. The Mössbauer spectrum at 80 K for the $Fe_{20}Cu_{40}Ag_{40}$ alloy, establishing its amorphous state. The solid lines are least-squares fits of the data, as discussed in the text.

A fourth candidate as an amorphous alloy is $Fe_{20}Cu_{40}Ag_{40}$, the alloy which had the broadest of all of the x-ray diffraction patterns. Its Mössbauer spectrum (figure 3) is a doublet, showing that it is paramagnetic. However, this does not necessarily mean that the iron atoms are dispersed in the fcc copper–silver lattice, as was the case in e.g. $Fe_{20}Cu_{80}$. Rather, it is possible that it is a ferromagnetic alloy whose Curie point is below room temperature. On cooling to 80 K the Mössbauer spectrum of this alloy becomes a broad sextet, with a proportion of the paramagnetic doublet remaining, as shown in figure 6. Analysis shows that the broad sextet has parameters similar to those of the other three alloys identified as amorphous (see table 1).

It is interesting to compare the Mössbauer data on these mechanically alloyed amorphous alloys with those reported for sputtered amorphous alloys. In figure 10 of their paper, Sumiyama *et al* [6] show the spectrum of a sputtered $Fe_{35}Cu_{33.5}Ag_{31.5}$ alloy which is similar in appearance to the spectrum obtained here for $Fe_{40}Cu_{30}Ag_{30}$. Secondary differences are apparent in the relative intensities of the lines in the Sumiyama spectrum, but this is attributable to the in-plane magnetic texture of the sputtered sample. The mean hyperfine field of the sputtered sample is given as 23.9 T. Although Sumiyama *et al* do not describe the model that they used to analyse their spectra, it is likely that the mean hyperfine-field parameter will be relatively model independent, as it largely corresponds to the degree of separation of the six lines. The mean hyperfine field of the mechanical alloys ranges from 25.2 T for $Fe_{40}Cu_{30}Ag_{30}$ to 17.6 T for $Fe_{33}Cu_{33}Ag_{33}$ and 13.8 T for $Fe_{30}Cu_{40}Ag_{30}$. As such it is clear that the mean hyperfine field of the sputtered alloy is a little higher than might have been expected given the trend in the mechanical alloy data, but not excessively so. More comprehensive Mössbauer data on the sputtered alloys are needed before any more

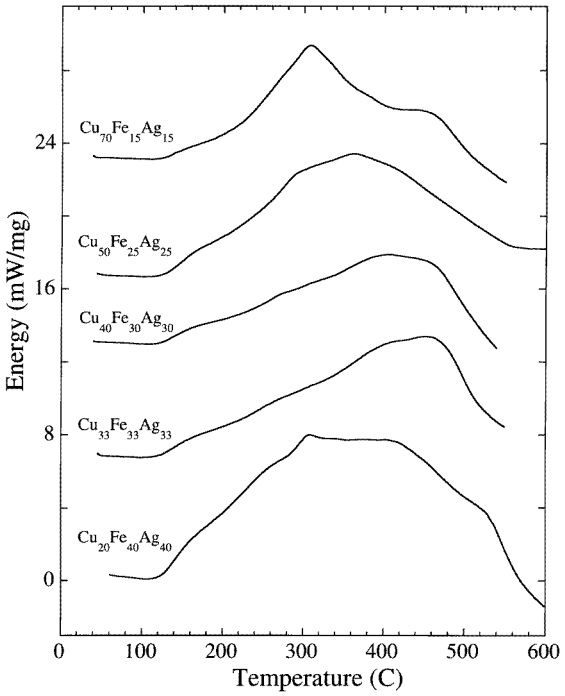

Figure 7. Differential scanning calorimetry curves for the ternary system $Cu_{100-2x}Fe_xAg_x$ for $x = 15$, 25, 30, 33.3 and 40. For clarity the curves have been offset from their true zeros by 27, 21, 16, 9 and 5 mW mg^{-1} respectively.

definite conclusions may be drawn from this comparison of the sputtered and mechanically alloyed states.

6. Differential scanning calorimetry

DSC data are shown in figure 7 for a series of $Cu_{100-2x}Fe_xAg_x$ samples. All show exothermic peaks in the range 150 to 550 °C, corresponding to the heat expelled by the alloy as the result of either decomposition or crystallization. A systematic variation in the curve shapes is seen. There is evidence of structure in the $x = 15$, 25 and 40 sample curves, with several peaks being superimposed in the vicinity of 300 to 500 °C. The two equi-proportioned alloys, with $x = 30$ and 33.3, have a more gradual response, starting at ∼150 °C, tending to a maximum at ∼400 or 450 °C, and returning towards zero by ∼550 °C. This is quite different from the DSC curves obtained for amorphous FeCuAg alloys made by sputtering, where a sharp peak was observed, centred at ∼130 °C [5]. In the sputtered alloys the existence of a sharp peak was interpreted as evidence for atomic scale amorphicity, where the onset of crystallization is sudden and uniform throughout the sample. By the same reasoning, the observed broad and featureless DSC curve for the ball-milled samples may be indicative of remanent crystallization on a very fine scale. If this were the case, then on heating the sample the crystallization process could occur gradually and/or inhomogeneously throughout the sample, without any sharp exothermic peaks in the DSC scan.

The residues of the DSC heating cycles were analysed by x-ray diffraction. In all cases polycrystalline and segregated Fe, Cu and Ag were found, with sharp XRD peaks indicating well crystallized phases.

Another feature of note in the DSC data is that variability was seen in the magnitude, but not the shape, of the curves recorded from different aliquots of the same sample batch. Differences of up to 30% were found in the exothermic heat given off from aliquots of both $Cu_{33}Fe_{33}Ag_{33}$ and $Cu_{70}Fe_{15}Ag_{15}$. It is not clear yet whether this was due to large-scale inhomogeneities in the samples, or an experimental problem.

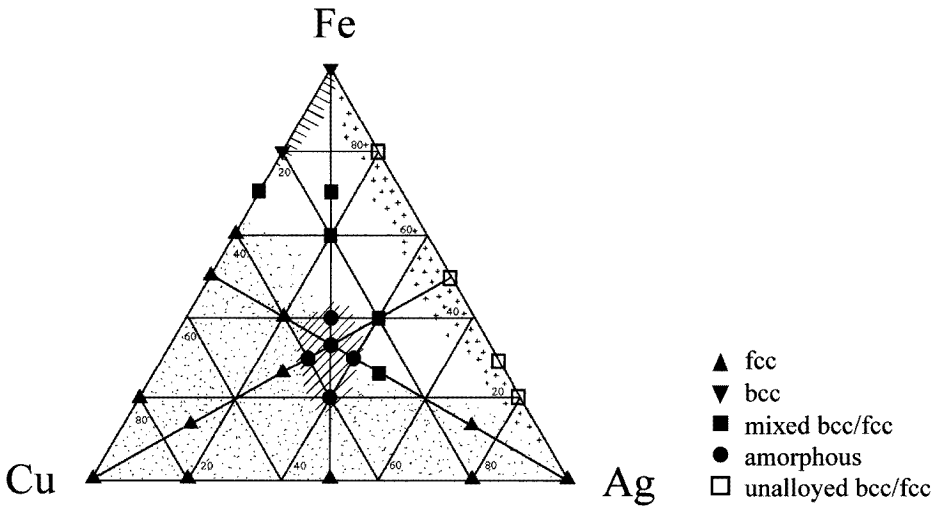

Figure 8. The ternary phase diagram of the mechanically alloyed FeCuAg system, summarizing the results of this study.

7. Conclusions

The ternary phase diagram of the ball-milled Fe–Cu–Ag system, as determined in this work, is shown in figure 8. We have shown that it is possible to produce metastable alloys with a range of structural and magnetic properties using mechanical alloying techniques, despite the natural immiscibility of the three elements. Data from x-ray diffraction and Mössbauer spectroscopy indicate that in those samples where alloying occurs, 70 hours' milling is sufficient to ensure completion.

In the binary Cu–Ag system, where both components have fcc lattices, a single-phase fcc solid-solution alloy results, irrespective of the starting composition. In the Fe–Cu system, with the added complication of different initial elemental structures, it was nevertheless possible to produce single-phase solid solutions. The structure is fcc when the iron concentration is below 60%, and bcc when it is above 80%. In the intermediate transition range, a mixed phase resulted. In the Fe–Ag system, the stored energy imparted during the milling process is insufficient for alloying to occur. The result is a microcrystalline mixture of elemental iron and silver particles, with a limited amount of intermetallic alloying. This structure has potential applications because of its giant magnetoresistive properties.

The ternary Fe–Cu–Ag system encompasses examples of single-phase, mixed-phase, and structurally disordered alloys, depending on the initial composition. The copper-

and silver-rich alloys have single-phase fcc structures. However, it is not possible to produce an equivalent iron-rich bcc alloy. The samples which contained approximately equal proportions of the starting elements were found to be highly disordered or amorphous as measured by Mössbauer spectroscopy. X-ray diffraction and differential scanning calorimetry data cast some doubt on there being a truly amorphous state at the atomic level, inferring that the samples retain some degree of crystallinity at very short-range length scales. However, in general the results compare favourably with those for sputter-deposited FeCuAg, where a similar but somewhat smaller amorphous region has been reported [5, 6].

Acknowledgments

We are grateful for the help of Marianne Odlyha and the University of London Intercollegiate Research Service in collecting the DSC data.

References

[1] Eckert J, Holzer J C, Krill C E and Johnson W L 1993 Mechanically driven alloying and grain size changes in nanocrystalline Fe–Cu powders *J. Appl. Phys.* **73** 2794–802
[2] Ma E, Atzmon M and Pinkerton F E 1993 Thermodynamic and magnetic properties of metastable Fe_xCu_{100-x} solid solutions formed by mechanical alloying *J. Appl. Phys.* **74** 955–62
[3] Wang J Q, Xiong P and Xiao G 1993 Investigation of giant magnetoresistance in concentrated and nanostructured alloys *Phys. Rev.* B **47** 8341–4
[4] Makhlouf S A, Sumiyama K, Wakoh K, Suzuki K, Takanashi K and Fujimori H 1993 Giant magnetoresistance of Fe-cluster-dispersed Ag films *J. Magn. Magn. Mater.* **126** 485–8
[5] Sumiyama K, Nishi K and Suzuki K 1991 Amorphous structure of the immiscible $Fe_{1-y}(Cu_{1-x}Ag_x)_y$ alloy system *J. Phys.: Condens. Matter* **3** 9859–69
[6] Sumiyama K, Yoshimoto K and Shiga M 1993 Hierarchy of non-equilibrium phases in the immiscible Fe–Cu–Ag alloy system *Acta Metall. Mater.* **41** 2487–95
[7] Lines M E and Eibschütz M 1983 Correlation effects in the Mössbauer spectra of amorphous metallic magnetic materials *Solid State Commun.* **45** 435–9
[8] Tanaka T, Nasu S, Huang B, Ishihara K N and Shingu P H 1993 Mössbauer spectroscopy of nanocrystalline pure iron prepared by mechanical milling *Nucl. Instrum. Methods* B **76** 195–6
[9] Butts A 1954 *Copper, the Metal, its Alloys and Components* (New York: Reinhold)
[10] Jiang J Z, Gonser U, Gente C and Bormann R 1993 Thermal stability of the unstable fcc-$Fe_{50}Cu_{50}$ phase prepared by mechanical alloying *Appl. Phys. Lett.* **63** 1056–8
[11] Hernando A, Crespo P, Barandiaran J M, Escorial A G and Yavari R 1993 Magnetic properties of mechanically alloyed Fe–Cu *J. Magn. Magn. Mater.* **124** 5–8
[12] Jiang J Z, Pankhurst Q A, Johnson C E, Gente C and Bormann R 1994 Magnetic properties of mechanically alloyed FeCu *J. Phys.: Condens. Matter* **6** L227–32
[13] Eilon M, Ding J and Street R 1995 Magnetic and magnetoresistive properties of mechanically alloyed $Fe_{25}Cu_{75}$ *J. Phys.: Condens. Matter* **7** 4921–8
[14] Eckert J, Holzer J C and Johnson W L 1993 Thermal stability and grain growth behavior of mechanically alloyed nanocrystalline Fe–Cu alloys *J. Appl. Phys.* **73** 131–41
[15] Macri P P, Rose P, Frattini R, Enzo S, Principi G, Hu W X and Cowlam N 1994 A study of $Cu_{50}Fe_{50}$ produced by mechanical alloying and its thermal treatment *J. Appl. Phys.* **76** 4061–7
[16] Jiang J Z and Chen F T 1994 A study of the microstructure of mechanically alloyed fcc-$Fe_{50}Cu_{50}$ *J. Phys.: Condens. Matter* **6** L343–8
[17] Massalski T B 1986 *Binary Alloy Phase Diagrams* (Metals Park, OH: American Society of Metals)
[18] Kataoka N, Sumiyama K and Nakamura Y 1985 Magnetic properties of high-concentration Fe–Ag alloys produced by vapour quenching *J. Phys. F: Met. Phys.* **15** 1405–11
[19] Kuyama J, Inui H, Imaoka S, Nasu S, Ishihara K N and Shingu P H 1991 Nanometer sized crystals formed by the mechanical alloying in the Ag–Fe system *Japan. J. Appl. Phys. Lett.* **30** L854–6
[20] Pankhurst Q A 1996 Iron-based amorphous ribbons and wires *Mössbauer Spectroscopy Applied to Magnetism and Magnetic Materials* vol 2, ed G J Long and F Grandjean (New York: Plenum) pp 59–83